AJNR Am J Neuroradiol 25:377–381, March 2004

Technical Note

Quantitative Assessment of Parenchymal and Ventricular Readjustment to Intracranial Pressure Relief

Christoph Preul, Marc Tittgemeyer, Dirk Lindner, Christos Trantakis, and Jürgen Meixensberger

Summary: A 26-year-old patient underwent endoscopic third ventriculostomy for the treatment of obstructive hydrocephalus. 3D volume data sets were obtained at 3 T before surgery and three times after surgery. Off-line analysis of individual imaging data (initial linear registration, intensity adjustment, and final nonlinear registration of pre- to postoperative MR images) yielded 3D displacement fields representing the postoperative structural brain change. In principle, such an analysis technique can be used in any clinical follow-up for which careful observation of tissue readjustment is of particular importance.

The adaptation of the brain parenchyma and ventricular system to altered intracranial pressure conditions is an important part of the evaluation of MR images. In the treatment of hydrocephalus, for instance, these changes can be vital when comparing pre- and postoperative ventricular size. We introduce a technique for visualizing and quantifying the dynamics of such tissue adaptation.

MR imaging provides a standard method in preoperative diagnostic performance to visualize the morphology of the third ventricle and its anatomic landmarks (1–5). The routine procedure of endoscopic third ventriculostomy bypasses a stenotic aqueduct or fourth ventricular outlet by windowing the third ventricular floor to deviate the CSF into the interpeduncular and prepontine cisterns (5–7). In the postoperative course, MR imaging is used to verify the patency of the stoma and to evaluate any ventricular adjustment (8–10). The readjustment of the ventricular system is one prominent parameter with which to document the success of the intervention, aside from clinical improvement (6, 8, 11).

The dynamics of textural and ventricular readjustment after intracranial pressure relief has not been largely investigated or visualized to date. We monitored such structural change by means of off-line image processing of subsequent MR images. The nonlinear mapping of these images onto one another yields the displacement vectors that reflect the structural change. A quantification of the displacement vectors can be enlisted as a criterion accompanying the clinical course and, thus, can aid in comprehension of the success or failure of the intervention.

Received April 10, 2003; accepted after revision August 26.

From the Max-Planck-Institute of Human Cognitive and Brain Science (C.P., M.T.) and the Klinik und Poliklinik für Neurochirurgie der Universität Leipzig (C.P., D.L., C.T., J.M.), Leipzig, Germany.

Address reprint requests to Christoph Preul, MD, Max-Planck-Institute of Human Cognitive and Brain Sciences, Stephenstrasse 1a, 04103 Leipzig, Germany.

© American Society of Neuroradiology

Technique

Deformation Field Analysis

To quantitatively estimate structural reconfiguration, we used a multi-step approach. First, the MR images were reoriented to the plane of anterior and posterior commissure. Upon reorientation, the images were processed for gray-scale normalization and removal of intensity inhomogeneities. Rigid registration was then applied to align objects in the images for position and orientation. A fuzzy C means the algorithm was used to segment the tissue types (12). To assess volumetric values for the ventricles, the lateral and third ventricles were segmented according to the procedure as introduced by Hojjatoleslami and Kruggel (13) and adapted by Schnack et al (14). After segmentation, the ventricular and cortical surfaces were generated as smooth triangular meshes, where brain substructures such as brain stem and cerebellum have been removed. Non-rigid registration was used to monitor residual differences between the images, which reflect morphologic, local changes. Because of the large deformations that originate from the neurosurgical approach, we based this registration on a fluid dynamic model (15, 16). The resulting vector field was then superimposed in a 1:1 size relation to the underlying MR image to render a direct measurement of change possible (Fig 3).

Standard Manual Planimetric Measures of the Ventricles

To assess the ventricular size, we measured a ventricular body index and the width of the third ventricle. The ventricular body index is the relation between the maximum distance of the lateral ventricles at the level of the ventricular body and the internal diameter of the skull at the same level and orientation. The third ventricle was measured at its maximum anterior widths.

Results

Clinical Case

A 26-year-old man presented to the neurosurgery clinic with subacute onset of attacks of headaches, vertigo, and nausea but without any focal neurologic deficits. Preoperative MR imaging revealed a lateral and third ventricular enlargement and showed evidence for an at least partially occluded aqueduct, suggesting noncommunicating triventricular hydrocephalus (Fig 1). Third ventricular bulging pushed the

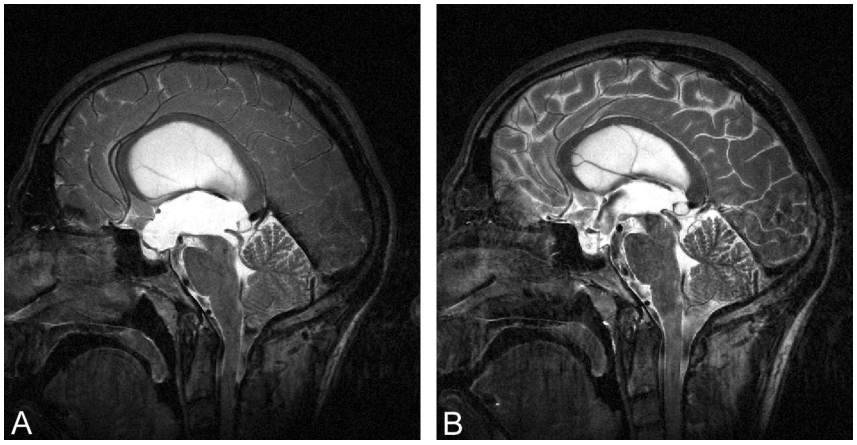

FIG 1. Sagittal view T2-weighted MR image (8500/80 [TR/TE]; section thickness, 3 mm), obtained at 3 T on a Bruker Medspec 30/100 system in the midsagittal plane, suggests tri-ventricular hydrocephalus due to aqueductal stenosis.

A, Third ventricular floor vaults toward the infundibular fossa.

B, Postoperative condition 8 months after surgery is shown.

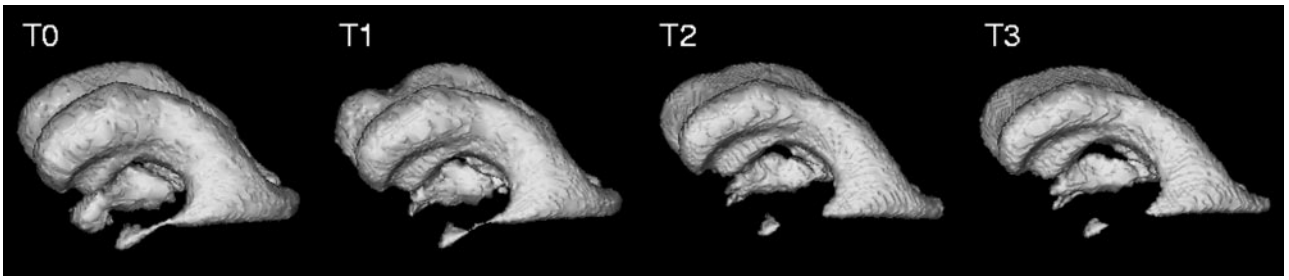

FIG 2. 3D rendering of the automatically segmented ventricular system during follow-up after endoscopic third ventriculostomy. The underlying 3D MR data sets were acquired preoperatively (T0) and postoperatively at 4 days (T1), 3 months (T2), and 8 months (T3) after the intervention. Measurement of the absolute ventricular volume yields 218, 177, 133, and 112 mL, respectively.

anterior recessus toward the infundibular fossa. Brain stem and pontine structures bent toward the clivus. The endoscopic procedure was performed through a right side paramedian coronal burr hole by using a rigid neuroendoscope. In situ inspection showed turbulent CSF flow between the third ventricular floor and the interpeduncular cistern after windowing the terminal membrane and a firm additional membrane underneath the real third ventricular floor. The patient totally recovered from his symptoms shortly after surgery.

Figure 1 shows the preoperative condition and the latest postoperative condition. The postoperative MR images were obtained 4 days, 3 months, and 8 months after the intervention and show readjustment of the ventricles and brain tissue to the altered intracranial pressure condition (Fig 2). Regarding the ventricular system, deformation analyses revealed an upward movement of the pontine and brain stem structures of 9 mm. The third ventricular floor, especially the terminal membrane, retreated from the infundibular recess for 5 mm. In addition, the whole ventricular roof descended 8.5 mm (Fig 3B and C). Planimetric measurement revealed a constant decrease of the ventricular body index and the third ventricular widths from 0.47 to 0.38 and from 19 mm to 12 mm, respectively. These values highly correlate with $r = 0.968$. The volume of the ventricles (lateral ventricles plus third ventricle) decreased by 49% from the preoperative to the latest postoperative MR image. Figure 2 suggests a continuous decrease of all ventricular compartments.

Figure 3 substantiates the underlying local shape differences in a color-coded visualization: for each point on the ventricular surface (Fig 3A) or brain surface (Fig 3B), the displacement vector is decomposed into its two components. One is perpendicular (normal) and the other tangential to the surface. If the normal component points inward, the shape difference is coded in red; conversely, the blue color corresponds to outward-pointing normals. The intensity of the respective color reflects the magnitude of the underlying displacement vector. The scale is presented in millimeters.

Additionally, a sparse set of the displacement vectors themselves is shown as arrows (with green stem, purple basis, and yellow arrowhead). Because the displacement vectors are defined at any voxel in the image volume, morphologic change can be visualized at any location within the brain. The capability of the vector field analysis is impressively shown at the third ventricular floor and at the region of the surgical approach, where the effect of the manipulation can be directly inferred (Fig 3B and C).

Discussion

The adjustment of the brain parenchyma and the ventricles to intracranial pressure conditions serves as one important morphologic indicator, in addition to the clinical course of the patient, for success or failure of CSF draining surgery. It has been shown in several studies that these two criteria do not necessarily coincide (5, 6, 8–10). In our opinion, the mere planimetric assessment of the ventricular size is inappropriate because it fails to reflect clinical improvement

due to subtle local changes. In this study, we present a method to visualize and quantify the dynamics of the remodeling process.

For the case presented herein, the pronounced changes in the surrounding of the third ventricle in the early postoperative image reflect acute adjustments of the tissue to the altered pressure condition. In contrast, only minor changes can be observed in the late postoperative images. We interpret this finding as chronic adaptations to the new balance of CSF circulation. Our findings match those reported by Schwartz et al (9), who stated that direct measurement of intracranial pressure reveals a decrease with a delay of 4 to 8 days postoperatively. Moreover, they hypothesized that ventricular volume might significantly decrease as early as the first 3 weeks after surgery. Our observations support this hypothesis in that we were able to show a 19% reduction of the ventricular volume as early as 4 days after surgery. During the next 3 months, the volume further decreased by 20%. After 8 months, the ventricular volume shrank another 10% (Fig 2). Accordingly, the third ventricle shows massive early reconfiguration, whereas the subtle adaptations characterize the later course.

We have shown that these adaptations can be appropriately visualized by means of displacement vectors. A quantification of the displacement vectors can be enlisted as a criterion accompanying the clinical course. This quantification can aid in comprehension of the success or failure of the intervention. We apply this technique at our department on a routine basis for all patients with hydrocephalus to assess postoperative changes. In principle, such analysis is applicable for any disease for which careful observations of subtle tissue changes are particularly important.

References

1. Ernestus RI, Krüger K, Ernst S, Lackner K, Klug N. **Relevance of magnetic resonance imaging for ventricular endoscopy.** *Minim Invasive Neurosurg* 2002;45:72–77
2. Morota N, Watabe T, Inukai T, Hongo K, Nakagawa H. **Anatomical variants in the floor of the third ventricle: implications for endoscopic third ventriculostomy.** *J Neurol Neurosurg Psychiatry* 2000;69:531–534
3. Rohde V, Gilsbach JM. **Anomalies and variants of the endoscopic anatomy for third ventriculostomy.** *Minim Invasive Neurosurg* 2000; 43:111–117
4. Vinas FC, Dujovny N, Dujovny M. **Microanatomical basis for the third ventriculostomy.** *Minim Invasive Neurosurg* 1996;39:116–121
5. Wilcock DJ, Jaspan T, Worthington BS, Punt J. **Neuro-endoscopic third ventriculostomy: evaluation with magnetic resonance imaging.** *Clin Radiol* 1997;52:50–54
6. Goumnerova LC, Frim DM. **Treatment of hydrocephalus with third ventriculocisternostomy: outcome and CSF flow patterns.** *Pediatr Neurosurg* 1997;27:149–152
7. Schroeder HW, Niendorf WR, Gaab MR. **Complications of endoscopic third ventriculostomy.** *J Neurosurg* 2002;96:1032–1040
8. Kulkarni AV, Drake JM, Armstrong DC, Dirks PB. **Imaging correlates of successful endoscopic third ventriculostomy.** *J Neurosurg* 2000;92:915–919
9. Schwartz TH, Ho B, Prestigiacomo CJ, Bruce JN, Feldstein NA, Goodman RR. **Ventricular volume following third ventriculostomy.** *J Neurosurg* 1999;91:20–25
10. Schwartz TH, Yoon SS, Cutruzzola FW, Goodman RR. **Third ventriculostomy: post-operative ventricular size and outcome.** *Minim Invas Neurosurg* 1996;39:122–129
11. Buxton N, Turner B, Ramli N, Vloeberghs M. **Changes in third ventricular size with neuroendoscopic third ventriculostomy: a blinded study.** *J Neurol Neurosurg Psychiatry* 2002;72:385–387
12. Wolters, CH. Influence of tissue conductivity inhomogeneity and anisotropy to EEG/MEG based source localization in the human brain [PhD Thesis]. Leipzig: University of Leipzig; 2003
13. Hojjatoleslami SA, Kruggel F. **Segmentation of large brain lesions.** *IEEE Trans Med Imaging* 2001;20:666–669
14. Schnack HG, Hulshoff HE, Baare WF, Viergever MA, Kahn RS. **Automatic segmentation of the ventricular system from MR images of the human brain.** *Neuroimage* 2001;14:95–104
15. Tittgemeyer M, Wollny G, Kruggel F. **Visualising deformation fields computed by non-linear image registration.** *Comput Visual Sci* 2002;5:45–51
16. Wollny G, Kruggel F. **Computational cost of non-rigid registration algorithms based on fluid dynamics.** *IEEE Trans Med Imaging* 2002;21:946–952

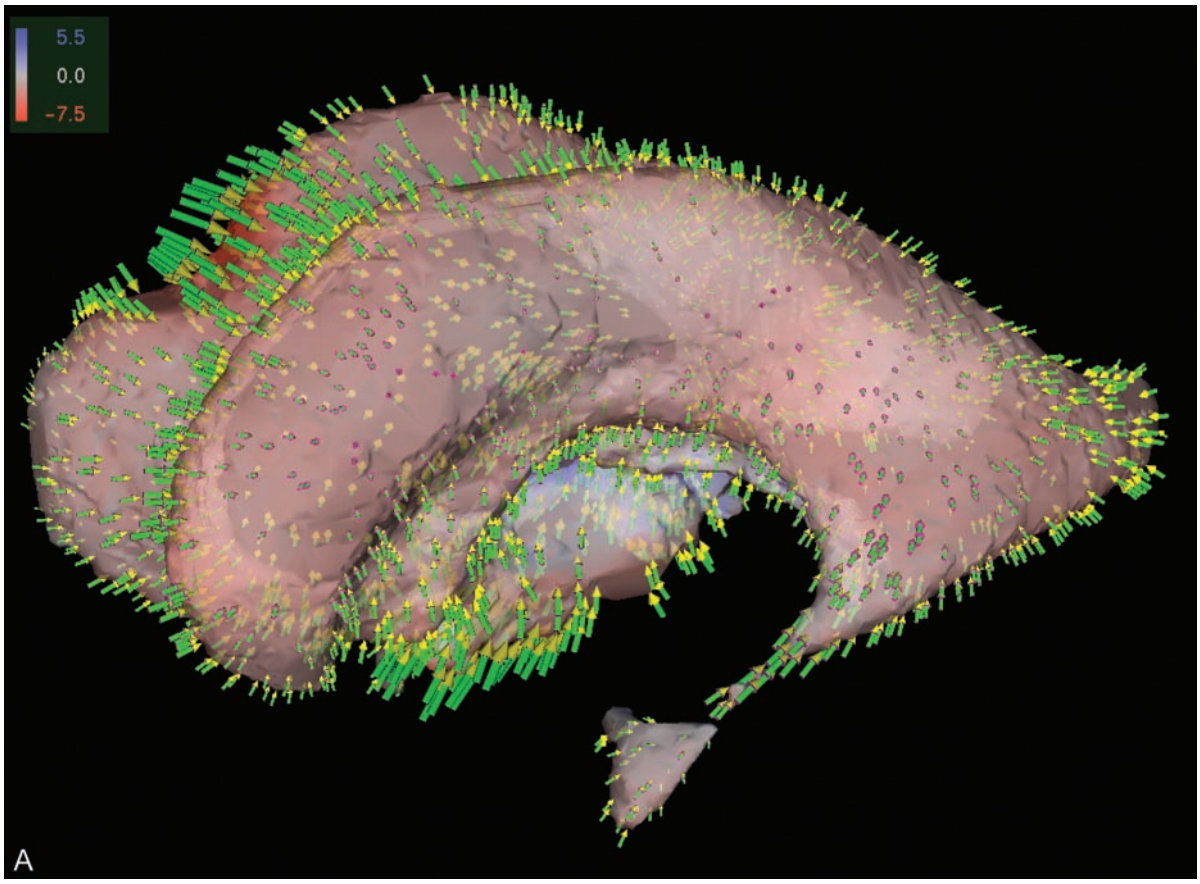
5.5
0.0
-7.5
A

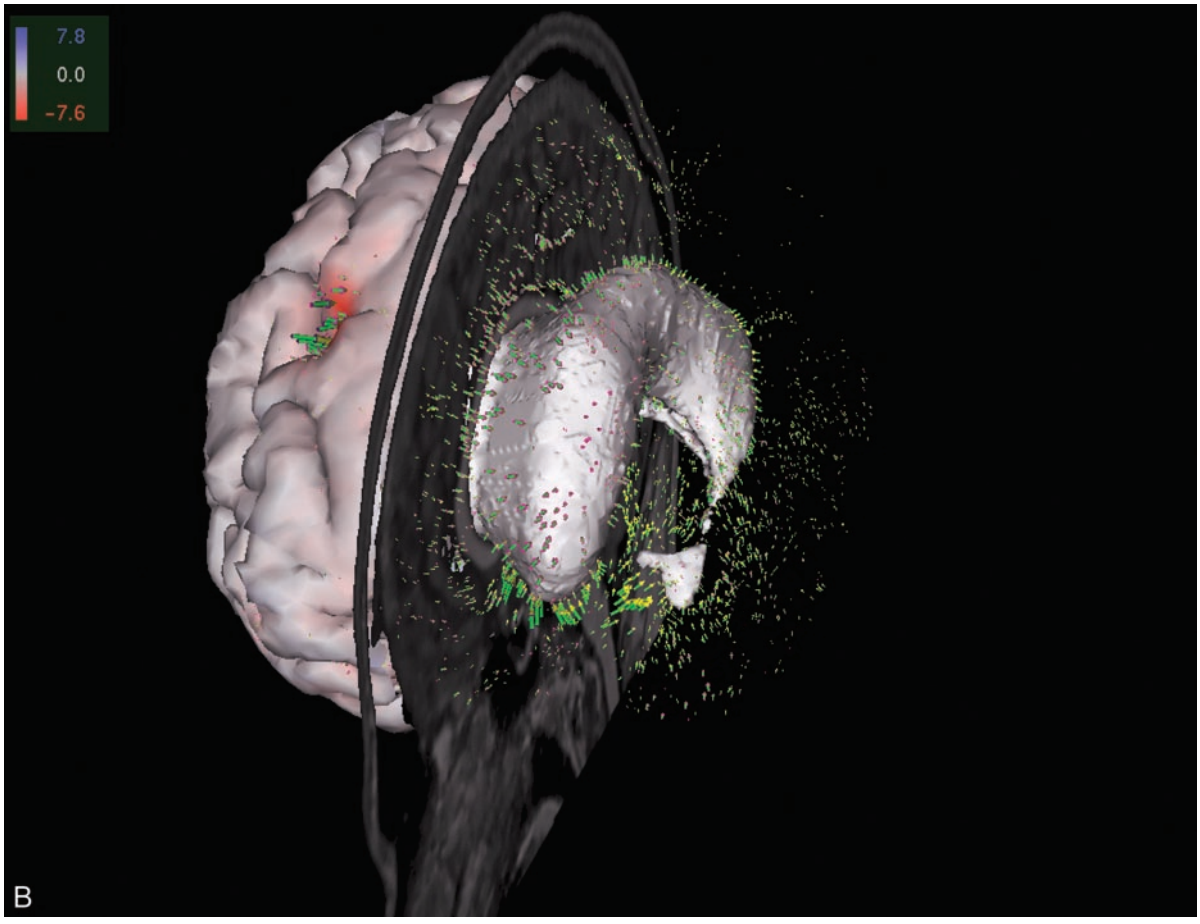
7.8
0.0
-7.6
B

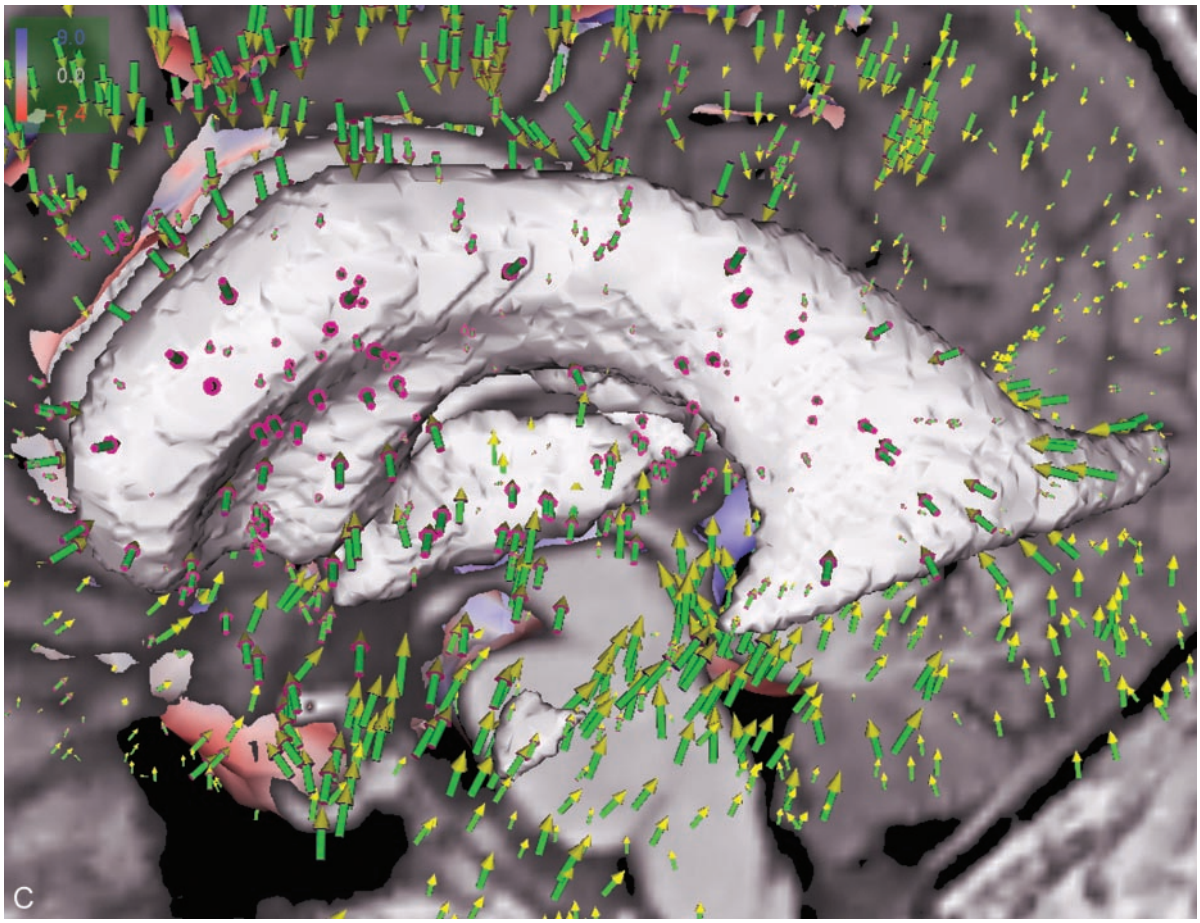

FIG 3. Shape difference of patient's ventricular system. *Colors* indicate orientation and magnitude of shape difference; *arrows* indicate displacements.

A, Preoperative versus early postoperative status.

B, Superposition of displacement field, segmented ventricular system, and latest postoperative image obtained at the midsagittal plane.

C, Detailed view into anatomy of third ventricle shows tissue adaptations to altered intracranial pressure condition.